



Cite this: *Chem. Commun.*, 2018, 54, 12045

Received 4th June 2018,
Accepted 26th September 2018

DOI: 10.1039/c8cc04464c

rs.c.li/chemcomm

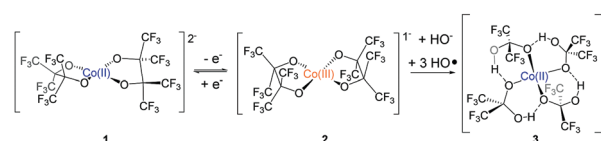
Square-planar Co(III) in {O₄} coordination: large ZFS and reactivity with ROS†

Jennifer L. Steele,^a Laleh Tahsini,^a Chen Sun,^a Jessica K. Elinburg,^a Christopher M. Kotyk,^a James McNeely,^a Sebastian A. Stoian,^b Alina Dragulescu-Andrasi,^d Andrew Ozarowski,^c M. Ozerov,^c J. Krzystek,^c Joshua Telser,^f Jeffrey W. Bacon,^a James A. Golen,^e Arnold L. Rheingold^e and Linda H. Doerrer^{ib}*^a

Oxidation of distorted square-planar perfluoropinacolate Co compound [Co^{II}(pin^F)₂]²⁻, **1**, to [Co^{III}(pin^F)₂]¹⁻, **2**, is reported. Rigidly square-planar **2** has an intermediate-spin, *S* = 1, ground state and very large zero-field splitting (ZFS) with *D* = 67.2 cm⁻¹; |*E*| = 18.0 cm⁻¹, (*E*/*D* = 0.27), *g*_⊥ = 2.10, *g*_∥ = 2.25 and $\chi_{\text{TIP}} = 1950 \times 10^{-6} \text{ cm}^3 \text{ mol}^{-1}$. This Co(III) species, **2**, reacts with ROS to oxidise two (pin^F)²⁻ ligands to form tetrahedral [Co^{II}(Hpfa)₄]²⁻, **3**.

Metal complexes supported by oxidatively robust ligands are crucial to many catalytic transformations including water remediation,¹ water oxidation,^{2–4} and selective C–H bond oxidation.^{5–8} One approach that engenders oxidative resistance is to use extensively fluorinated ligands. Chelating bidentate ligands have additional stability vs. two monodentate ligands, and H₂pin^F, perfluoropinacol, is of particular interest because its complexes can routinely be prepared in water (p*K*_{a1} = 6.05, p*K*_{a2} = 10.7, titration in Fig. S1, ESI†). Homoleptic 3d complexes [M(pin^F)₂]²⁻ with M = Fe–Zn have been reported^{9,10} including [Me₄N]₂[Co(pin^F)₂], **1** (Scheme 1), which binds CH₃CN but not THF in solution.¹⁰ Reactivity with O₂ for this Co species was also reported,¹¹ the conclusions from which we have come to doubt as discussed below.

Compound **1** is stable for days in aqueous solutions as the five coordinate adduct [Co(OH₂)(pin^F)₂]²⁻ when buffered between



Scheme 1 Formal interconversions of anions [Co(pin^F)₂]²⁻, **1**, [Co(pin^F)₂]¹⁻, **2**, and [Co(Hpfa)₄]²⁻, **3**.

pH 9–11 with (pin^F)²⁻.¹² In contrast, CH₃CN solutions of **1** in air undergo distinct colour changes in hours. The pink **1** (λ_{max} , nm (ϵ , M⁻¹ cm⁻¹) = 505 (27), 560 (43), converts to a bright yellow/orange species with an intense absorption at 405 nm (3790), **2**, and then ultimately transforms to a violet species, **3** (λ = 481 (133), 567 (165)) in ~95% yield after five days (Fig. S2, ESI†). Purple X-ray quality crystals were obtained by layering Et₂O onto violet acetone solutions, enabling identification of the pseudo-tetrahedral complex [Me₄N]₂[Co^{II}(Hpfa)₄], **3**. The metal centre is bound by four monodentate alkoxide ligands, designated (Hpfa)⁻ for the monodeprotonated form of the perfluoroacetone geminal diol, H₂pfa (Scheme 1 and Fig. 1).

As noted, the conversion of **1** to **3** in CH₃CN under aerobic conditions passes through an orange intermediate, **2**, with a strong absorbance at 405 nm. Efforts to isolate the orange species from this reaction mixture were unsuccessful. The composition of **3** suggests that four equiv of hydroxyl radical, HO•, are formally required for its formation (see Scheme S1, ESI†). Therefore, we treated **1** with H₂O₂ trying to prepare a posited {Co(III)–OH} species. Adding one equiv of H₂pin^F to **1** in wet CH₃CN, followed by one equiv of H₂O₂, affords an absorbance increase at 405 nm over an hour (Fig. 2). Next, the ligand-cleaved product **3** can be formed by adding one equiv of Me₄NOH to **2** following its full formation (Fig. S3, ESI†). Isolation of a posited Co(III) intermediate was not achieved from this reaction, due to an additional pathway that led to an insoluble brown solid and complete loss of product after 24 h. Conversion of **1** to **2** occurs at a faster rate in the presence of larger amounts of hydrogen peroxide.

Analytically pure **2** was obtained by oxidizing **1** under N₂ with AgPF₆ in THF/CH₃CN to yield the surprising square-planar

^a Chemistry Department, Boston University, 590 Commonwealth Ave., Boston, MA 02215, USA. E-mail: doerrer@bu.edu

^b Department of Chemistry, University of Idaho, 875 Perimeter Drive, MS 2343, Moscow, ID 83844, USA

^c National High Magnetic Field Laboratory, Florida State University, 1800 E. Paul Dirac Drive, Tallahassee, FL 32310, USA

^d Department of Chemistry and Biochemistry, Florida State University, 95 Chieftan Way, Tallahassee, FL 32306, USA

^e Department of Chemistry and Biochemistry, University of California, San Diego, 9500 Gilman Drive, MC 0332, La Jolla, CA 92093, USA

^f Department of Biological, Chemical and Physical Sciences, Roosevelt University, Chicago, IL 60605, USA

† Electronic supplementary information (ESI) available. CCDC 1407677 (**2**) and 1407676 (**3**). For ESI and crystallographic data in CIF or other electronic format see DOI: 10.1039/c8cc04464c

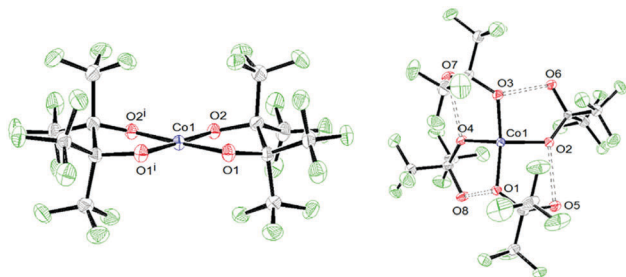


Fig. 1 ORTEPs of anions of **2** (left) and **3** (right). Dotted lines indicate hydrogen bonding interactions.

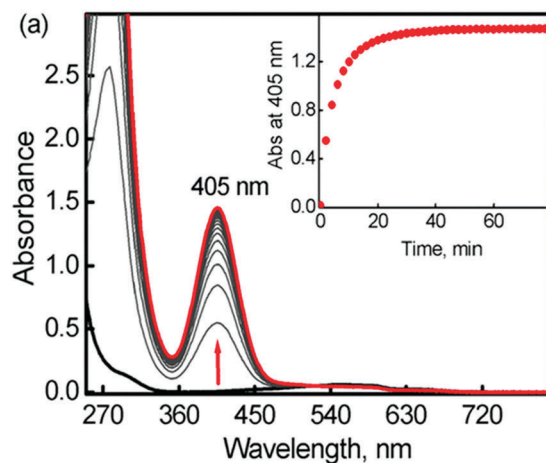


Fig. 2 UV-vis spectral changes of conversion of **1** to **2** effected by H_2O_2 in CH_3CN solution. Inset shows the time course of this process.

Co(III) species $[\text{Me}_4\text{N}][\text{Co}^{\text{III}}(\text{pin}^{\text{F}})_2]$. The UV-vis spectrum of **2** in CH_3CN has an LMCT band at $\lambda_{\text{max}} = 405 \text{ nm}$ ($\epsilon = 3790 \text{ M}^{-1} \text{ cm}^{-1}$). The solution-based, Evans method^{13–15} room-temperature magnetic moment of $3.63 \mu_{\text{B}}$ for **2** suggests an $S = 1$, intermediate-spin state. This observation is consistent with other Co(III) square planar compounds with $\{\text{N}_4\}$,^{16–19} $\{\text{S}_4\}$,^{20,21} $\{\text{C}_4\}$,²² and heteroleptic²³ coordination (summary in Table S1, ESI[†]). X-ray quality crystals were obtained by layering a THF solution onto CH_2Cl_2 (Fig. 1 and Table S3, ESI[†]). The square planar coordination with $\tau_4 = 0.03$ has Co–O bond lengths (1.8020(17) and 1.7995(18) Å) shorter than the average (1.962(3) Å) in **1**, as expected.¹⁰ Notably, the UV-vis spectra in both coordinating and non-coordinating solvents are virtually identical (Fig. S4, ESI[†]), indicating that there is no axial ligand bound in **2** in solid state or in solution. Even when hydroxide is added to **2**, no coordination is observed, suggesting a steric, not electronic, reason for unsaturation. The combination of shorter Co–O bonds and the steric bulk of eight CF_3 groups is proposed to inhibit coordination of a fifth ligand.

Addition of O_2 to $[\text{Bu}_4\text{N}]_2[\text{Co}(\text{pin}^{\text{F}})_2]$ in “acidified” solution has previously been reported to give a product with a λ_{max} of 405 nm.¹¹ Therein the product was proposed to be the high-spin cobalt(II) species $[\text{Bu}_4\text{N}][\text{Co}(\text{pin}^{\text{F}})(\text{Hpin}^{\text{F}})(\text{O}_2)] \cdot \text{EtOH}$ based on a solution magnetic moment measurement and EPR data.¹¹ Our attempts to repeat the isolation of this product by this

method have proved unsuccessful. Because **2** has an identical λ_{max} , similar light sensitivity, and similar magnetic moment to that reported earlier,¹¹ we suggest that the proposed formula¹¹ is incorrect, and that the previously reported compound was $(\text{Bu}_4\text{N})^+$ salt of $[\text{Co}^{\text{III}}(\text{pin}^{\text{F}})_2]^{1-}$.

Compound **2** incorporates a rare, paramagnetic Co(III) ion. The room-temperature $^1\text{H-NMR}$ -derived magnetic moment of **2** is corroborated by SQUID magnetometry on a solid sample. Fig. 3 shows $\chi T \sim 1.8 \text{ cm}^3 \text{ K mol}^{-1}$ at 300 K corresponding to an apparent effective magnetic moment of $3.78 \mu_{\text{B}}$. These values are intermediate between those expected for a triplet ($\chi T \approx 1 \text{ cm}^3 \text{ K mol}^{-1}$) and a quintet spin state ($\chi T \approx 3 \text{ cm}^3 \text{ K mol}^{-1}$). From 300 to 50 K, χT gradually decreases, followed by a more dramatic fall to nearly zero at very low temperature. This behaviour suggests the presence of a large temperature independent paramagnetic (TIP) contribution and a large zero-field splitting (ZFS) at low temperature. Least squares fitting of experimental data yielded a ZFS such that $|D| \sim 70 \text{ cm}^{-1}$, $E/D \sim 1/3$, $g_{\text{iso}} = 2.24$ and $\chi_{\text{TIP}} = 1950 \times 10^{-6} \text{ cm}^3 \text{ mol}^{-1}$. The observation of a triplet ground state with this large ZFS is corroborated by reduced magnetization data (inset of Fig. 3 and Fig. S5, ESI[†]), and lack of an EPR signal, regardless of temperature, even for frequencies as high as 600 GHz ($h\nu = 20 \text{ cm}^{-1}$).²⁴ The ZFS was directly measured by FIRMS (Far InfraRed Magnetic Spectroscopy),²⁵ which detected two resonances in zero field at 49.2 cm^{-1} and 85.2 cm^{-1} , identified as $D - E$ and $D + E$ transitions, respectively (Fig. 4) and leading to $|D| = 67.2 \text{ cm}^{-1}$; $|E| = 18.0 \text{ cm}^{-1}$. The $2E$ transition, which should appear at 36 cm^{-1} , was not observed and therefore the sign of D is likely to be positive. The positive sign of D is also supported by magnetic fits (Fig. S5, ESI[†]) and is predicted by second-order perturbation theory using the electronic structure discussed below. Together these observations reveal a large unquenched orbital momentum and a spin–orbit mixing of the orbital ground state with several low-lying orbital excited states.

To illuminate the nature of the paramagnetic ground state and to rationalize the observed spectroscopic behaviour, we have

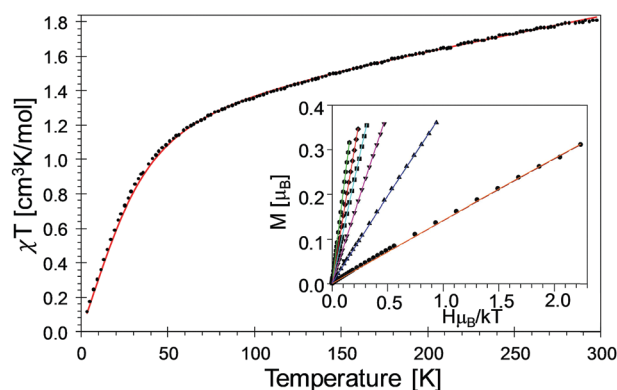


Fig. 3 Plot of χT vs. temperature recorded for a powder sample of **2**. Shown in black are experimental data points. The solid red line is a simulation obtained for $S = 1$ with $D = 70 \text{ cm}^{-1}$, $E/D = 0.33$, $g_{\text{iso}} = 2.24$, and $\chi_{\text{TIP}} = 1950 \times 10^{-6} \text{ cm}^3 \text{ mol}^{-1}$. The inset shows the reduced magnetization data recorded at 1.7 K, 5 K, 10 K, 15 K, 20 K, and 30 K for fields from 0 to 7 T. The solid lines are simulations obtained using $D = 65.44 \text{ cm}^{-1}$, $E/D = 0.33$, $g_{\text{iso}} = 2.22$.

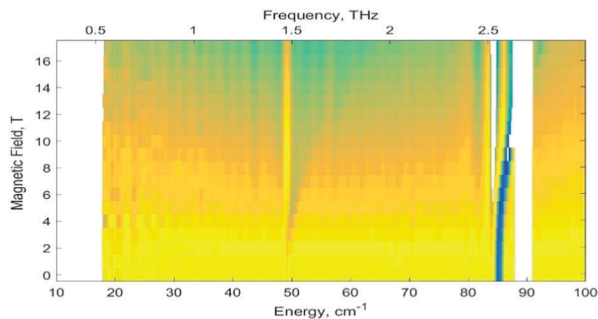
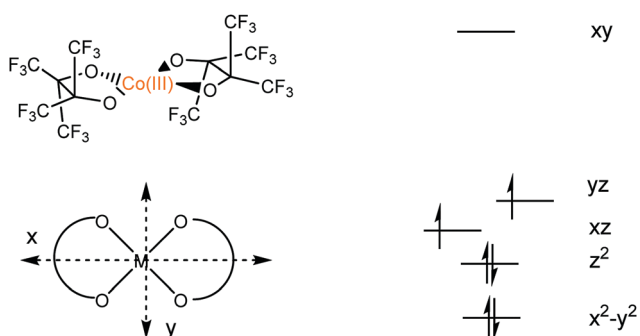


Fig. 4 A false colour map of FIRMS resonances at 5 K showing two zero-field transitions at 49.2 cm⁻¹ and 85.2 cm⁻¹ evolving into powder patterns with applied magnetic field. More details can be found in Fig. S6 and S7 in the ESI.†

completed a detailed theoretical investigation of **2**. Calculations using ORCA²⁶ revealed the ligand field splitting shown qualitatively in Scheme 2 (right).

An intermediate-spin, triplet ground state is further supported by triplet (³2, 0.0 kcal mol⁻¹), singlet (¹2, 38.9 kcal mol⁻¹), and quintet (⁵2, 15.8 kcal mol⁻¹) structures optimized at the PBE0/cc-pVTZ/RIJCOSX level of theory. These calculations not only yield a triplet configuration lowest in energy, but a geometry-optimized structure with the best structural agreement with **2** (Table S4, ESI†). The spin density for ³2 is localized on the Co atom (Fig. S8, ESI†) with the SOMOs best described as 3d_{xz} and 3d_{yz} orbitals. Analysis of the electron distribution suggests that the 3d_{z²} and 3d_{x²-y²} orbitals are doubly occupied and that, to a first approximation, the |(x² - y²)²(z²)²(xz)^z(yz)^z| Slater determinant describes best the ground state of **2**. This electronic structure is confirmed by NEVPT2(12,10) calculations (Fig. S14, ESI†). The cobalt spin population was 1.80/1.94 in the PBE0/NEVPT2(12,10) calculations for **2** and 1.80/1.95 for ³2 based on Löwdin population analysis. This result is a similar electronic structure to that reported in Co complexes with redox-active benzene dithiolate²⁷ and aminophenolate ligands.²⁸

To predict magnetic properties, NEVPT2 calculations were performed on top of CASSCF(12,10) references averaged over the three lowest triplet roots for **2** (see ESI†). The axial ZFS parameter *D*, rhombicity ratio *E/D*, and isotropic *g*-value were



Scheme 2 Coordinate system used for the discussion of **2** along with a qualitative ligand field splitting diagram derived from NEVPT2(12,10) calculations averaged over three triplet states. Natural orbitals can be found in Fig. S26 (ESI†).

calculated to be 77.1 cm⁻¹, 0.27, and 2.37 respectively. These theoretical values compare well with experiment. The *g*-tensor was calculated to be highly anisotropic with principal components *g_z* = 2.00, *g_x* = 2.43, and *g_y* = 2.67. The ³B₂ state (*D*₂ symmetry, 2273 cm⁻¹) is dominated by configurations characterized by 3d_{z²} to 3d_{xz} (72.0%) and 3d_{x²-y²} to 3d_{xz} (22.1%) excitations. The ³B₃ state's (3802 cm⁻¹) dominant configurations are characterized by 3d_{z²} to 3d_{yz} (72.0%) and 3d_{x²-y²} to 3d_{yz} (22.1%) excitations.

These quantum chemical theory calculations were complemented by a series of classical ligand field theory calculations²⁹ that determined *D* ≈ 70 cm⁻¹ with evidence that contributions from both quintet and singlet excited states are required for quantitative agreement with experiment, but the dominant contribution is from triplet excited states arising from transitions from the 3d_{z²} and 3d_{x²-y²} orbitals to the 3d_{xz} and 3d_{yz} orbitals (details in ESI†).

To understand the formation of **3** via **2**, **1** was reacted with O₂, H₂O, and H₂O₂. Compound **1** is stable up to pH = 11,¹² and therefore nucleophilic attack by hydroxide alone does not lead to C-C bond cleavage in neutral water; some oxidation is required. There is no appearance of **2** or conversion to **3** from the addition of H₂O or O₂ alone to **1**, but **1** reacts with O₂ in the presence of a mild acid such as H₂pin^F. This reaction slowly afforded **2**, but in significant yield only after four days, and complete conversion to **3** took seven days (Fig. S17, ESI†). When **2** in dry CH₃CN is exposed to air in the presence of (t^{Bu}₄N)PF₆, it is slowly converted to **3** as indicated by UV-vis spectroscopy (Fig. S18, ESI†), with a competing pathway leading to an insoluble brown precipitate. Starting with dry CH₃CN and gradual exposure to air, the conversion from **2** to **3** takes up to a month and also shows conversion to a transient Co(II) species after 24 h. This Co(II) species could be **1**, which is produced from a solution of **2** when exposed to light under N₂ (Fig. S18, ESI†). These observations suggest that both the oxidant O₂ and a source of H⁺ are necessary for the formation of **2**, and a further ROS (reactive oxygen species) is needed to form **3**. The fact that **2** does not form in H₂O suggests a radical species whose lifetime is greater in CH₃CN than H₂O.

Isotopic labelling experiments were conducted to determine the source of the new OH groups in the (Hpfa)⁻ ligands. Each of ¹⁸O₂ and H₂¹⁸O was separately introduced to a solution of **1**, while the other component was kept unlabelled, and **3** formed in CH₃CN. The product **3** was recrystallized and analysed by ESI-MS (Fig. S19–S21, ESI†) which showed ¹⁸O in [Co(Hpfa)₄]²⁻ from both reactions. These data and the H₂O₂ experiment suggest a reactive oxygen species (ROS), such as HO•, that can form in more than one way. Because oxidation is required, O₂ could be responsible for HO• formation, either indirectly from water oxidation, or directly from itself being converted to hydroxyl radical (Scheme S1, ESI†).

Redox behaviour was also investigated with cyclic voltammetry (CV). Compound **1** showed a quasi-reversible Co³⁺/Co²⁺ couple with an *E*_{1/2} of -0.134 V vs. Fc⁺/Fc (Fig. S22, ESI†). Under N₂, **2** showed a reversible couple with an *E*_{1/2} of -0.167 V vs. Fc/Fc⁺, and when **3** was studied in dry CH₃CN under N₂,

a widely-separated redox couple is observed, as well as another oxidation event (Fig. S23, ESI[†]).

The reactivity of these species was monitored by cyclic voltammetry. In CH₃CN under ambient conditions both electrochemical and UV-vis data confirm the completion of the reaction of **1** to **3** within several hours (Fig. S24, ESI[†]). However, under ambient conditions in CH₃CN no conversion of purified **2** to **3** was observed within one day, which is consistent with our previously noted UV-vis experiments.

Interestingly, the CV of **3** in wet CH₃CN shows oxidative catalytic current (Fig. S25, ESI[†]), which increases with subsequent additions of H₂O until a solid blue precipitate forms. Controlled potential electrolysis shows that the initial oxidative current significantly diminished after 750 s, and did not increase when H₂O was added at 1800 s. When the working electrode was placed in fresh electrolyte (Fig. S26 and S27, ESI[†]) little activity was observed indicating that there was no active heterogeneous film. This catalytic activity may be water oxidation by nanoparticulate CoO_x material, a known H₂O oxidation catalyst,³⁰ for which **3** is a precursor in CH₃CN. Little change was observed in CV data when the solution was filtered (Fig. S28, ESI[†]).

In summary, a highly unusual square-planar, paramagnetic Co(III) species, [Co(pin^F)₂]¹⁻, **2**, has been prepared from [Co(pin^F)₂]²⁻ by two different routes. Compound **2** has an intermediate-spin, *S* = 1, ground state and very large ZFS with $|D| = +67.2 \text{ cm}^{-1}$, $E/D = 0.27$, $g_{\perp} = 2.10$, $g_{\parallel} = 2.25$ and $\chi_{\text{TIP}} = 1950 \times 10^{-6} \text{ cm}^3 \text{ mol}^{-1}$. This compound reacts with reactive oxygen species to form a new tetrahedral Co(II) compound, [Co(Hpfa)₄]²⁻, **3**, encapsulated by four intramolecular hydrogen bonds among four monodentate diolate ligands.

This work was supported by NSF-CHE-1362550 (LHD), DOE-BES DE-FG02-11ER16253 (LHD), Boston University UROP, NSF-CHE-0619339 (BU NMR spectrometer). A portion of this work was performed at the National High Magnetic Field Laboratory, which is supported by National Science Foundation Cooperative Agreement No. DMR-1644779 and the State of Florida. Partial support for AD-A from the NSF (CHE-1464955) and the University of Idaho (SAS) is acknowledged. We thank the referees for useful mechanistic discussions.

Conflicts of interest

There are no conflicts to declare.

Notes and references

- 1 T. J. Collins and A. D. Ryabov, *Chem. Rev.*, 2017, **117**, 9140–9162.
- 2 H. Lv, Y. V. Geletii, C. Zhao, J. W. Vickers, G. Zhu, Z. Luo, J. Song, T. Lian, D. G. Musaev and C. L. Hill, *Chem. Soc. Rev.*, 2012, **41**, 7572–7589.
- 3 J. J. Concepcion, J. W. Jurss, M. K. Brennaman, P. G. Hoertz, A. O. T. Patrocínio, N. Y. Murakami Iha, J. L. Templeton and T. J. Meyer, *Acc. Chem. Res.*, 2009, **42**, 1954–1965.
- 4 P. Du and R. Eisenberg, *Energy Environ. Sci.*, 2012, **5**, 6012–6021.
- 5 R. A. Sheldon, I. W. C. E. Arends, G.-J. ten Brink and A. Dijkstra, *Acc. Chem. Res.*, 2002, **35**, 774–781.
- 6 D. Wang, A. B. Weinstein, P. B. White and S. S. Stahl, *Chem. Rev.*, 2018, **118**, 2636–2679.
- 7 S. R. Neufeldt and M. S. Sanford, *Acc. Chem. Res.*, 2012, **45**, 936–946.
- 8 B. G. Hashiguchi, S. M. Bischof, M. M. Konnick and R. A. Periana, *Acc. Chem. Res.*, 2012, **45**, 885–898.
- 9 S. A. Cantalupo, S. R. Fiedler, M. P. Shores, A. L. Rheingold and L. H. Doerrer, *Angew. Chem., Int. Ed.*, 2012, **51**, 1000–1005.
- 10 L. Tahsini, S. E. Specht, J. S. Lum, J. J. M. Nelson, A. F. Long, J. A. Golen, A. L. Rheingold and L. H. Doerrer, *Inorg. Chem.*, 2013, **52**, 14050–14063.
- 11 C. J. Willis, *J. Chem. Soc., Chem. Commun.*, 1974, 117–118.
- 12 L. Tahsini, W. P. Carbery, M. Z. Ertem, S. A. Cantalupo, J. A. Golen, A. L. Rheingold, V. S. Batista and L. H. Doerrer, 2018, manuscript in preparation.
- 13 G. A. Bain and J. F. Berry, *J. Chem. Educ.*, 2008, **85**, 532–536.
- 14 D. F. Evans, *J. Chem. Soc.*, 1959, 2003–2005.
- 15 S. K. Sur, *J. Magn. Reson.*, 1989, **82**, 169–173.
- 16 S. E. Harnung and E. Larsen, *Inorg. Chem.*, 2007, **46**, 5166–5173.
- 17 B. Ramdhanie, L. N. Zakharov, A. L. Rheingold and D. P. Goldberg, *Inorg. Chem.*, 2002, **41**, 4105–4107.
- 18 L. H. Doerrer, M. T. Bautista and S. J. Lippard, *Inorg. Chem.*, 1997, **36**, 3578–3579.
- 19 P. J. M. W. L. Birker, J. J. Bour and J. J. Steggerda, *Inorg. Chem.*, 1973, **12**, 1254–1259.
- 20 R. Williams, E. Billig, J. H. Waters and H. B. Gray, *J. Am. Chem. Soc.*, 1966, **88**, 43–50.
- 21 F. L. Benedito, T. Petrenko, E. Bill, T. Weyhermüller and K. Wieghardt, *Inorg. Chem.*, 2009, **48**, 10913–10925.
- 22 M. A. Garcia-Monforte, I. Ara, A. Martín, B. Menjón, M. Tomás, P. J. Alonso, A. B. Arauzo, J. I. Martínez and C. Rillo, *Inorg. Chem.*, 2014, **53**, 12384–12395.
- 23 P. O. Lagaditis, B. Schluschaß, S. Demeshko, C. Würtele and S. Schneider, *Inorg. Chem.*, 2016, **55**, 4529–4536.
- 24 A. K. Hassan, L. A. Pardi, J. Krzystek, A. Sienkiewicz, P. Goy, M. Rohrer and L.-C. Brunel, *J. Magn. Reson.*, 2000, **142**, 300–312.
- 25 J. Ludwig, Y. B. Vasilyev, N. N. Mikhailov, J. M. Poumirol, Z. Jiang, O. Vafek and D. Smirnov, *Phys. Rev. B*, 2014, **89**, 241406.
- 26 F. Neese, *Wiley Interdiscip. Rev.: Comput. Mol. Sci.*, 2012, **2**, 73–78.
- 27 K. Ray, A. Begum, T. Weyhermüller, S. Piligkos, J. van Slageren, F. Neese and K. Wieghardt, *J. Am. Chem. Soc.*, 2005, **127**, 4403–4415.
- 28 B. Eckhard, E. Bothe, P. Chaudhuri, K. Chlopek, D. Herebian, S. Kokatam, K. Ray, T. Weyhermüller, F. Neese and K. Wieghardt, *Chem. – Eur. J.*, 2005, **11**, 204–224.
- 29 J. Bendix, in *Comprehensive Coordination Chemistry II, Fundamentals: Physical Methods, Theoretical Analysis, and Case Studies*, ed. A. B. P. Lever, Elsevier, Amsterdam, 2003, vol. 2, pp. 673–676.
- 30 X. Deng and H. Tuysuz, *ACS Catal.*, 2014, **4**, 3701–3714.